Electronic and Structural Elements that Regulate the Excited-State Dynamics in Purine Nucleobase Derivatives

Carlos E. Crespo-Hernández,*[,a] Lara Martínez-Fernández,[†,b] Clemens Rauer,[†, c] Christian Reichardt,[†,a] Sebastian Mai,[c] Marvin Pollum,[a] Philipp Marquetand,[c] Leticia González,*[,c] and Inés Corral*[,b]

[a] Department of Chemistry and Center for Chemical Dynamics, Case Western Reserve University, 10900 Euclid Avenue, Cleveland, Ohio 44106 USA

[b] *Departamento de Química, Facultad de Ciencias, Universidad Autónoma de Madrid, Campus de Excelencia UAM-CSIC, Módulo 13, Cantoblanco, 28049 Madrid, Spain*

[c] *Institute of Theoretical Chemistry, University of Vienna, Währinger Str. 17, 1090 Vienna, Austria*

Supporting Information

I. EXPERIMENTAL METHODS & SUPPORTING RESULTS

1. Chemicals. 9-Methylpurine (99%) and purine free base (≥ 98.5%) were obtained from HDH Pharma, Inc. (San Diego, CA) and from Sigma-Aldrich, respectively. Cyclohexane (99.9%) and acetonitrile (99.6%) were obtained from Fisher Scientific. Chloroform (99.8%) was obtained from Sigma-Aldrich. All chemicals were used as received. Water was obtained from a water ultra purification system (Barnstead International, Dubuque, IA). Phosphate buffer solutions were freshly prepared using 0.24 g of sodium dihydrogen phosphate and 0.177 g of disodium hydrogen phosphate dissolved in 200 mL of ultrapure water and adjusted to pH 7.

2. Assignment of Steady-State Absorption and Emission Spectra. Previous investigations have shown that the absorption spectrum of purine in the spectral region from ~185 to 340 nm in water,[1,2] methylcyclohexane,[3,4] and trimethylphosphate,[3] is composed of four to five electronic transitions of ππ* and nπ* character. The assignment of the absorption spectrum of the purine free base is complicated by the presence of these multiple ^{1}ππ* and ^{1}nπ* electronic transitions [1-9] and also by the co-existence of the N7H and N9H tautomers in solution.[10-14] On

DOI: 10.1021/ja512536c
J. Am. Chem. Soc. **2015**, S1

the one hand, NMR[10,11] and resonance Raman[12,13,15] experiments have concluded that both the N7H and N9H tautomers co-exist in approximately equal ratio in aqueous solution, with a slight predominance of the N7H tautomer. On the other hand, the N9H tautomer is more abundant in aprotic and nonpolar solvents[7,8,10,11] and is considered to be the principal species in the gas phase.[16-20] Methylation of the purine free base at the N9 position can simplify the assignment of the absorption spectrum of the purine chromophore by removing prototropic tautomerism from the equation.[1,6]

As in the adenine and guanine monomers,[21,22] the strong absorption band centered around 260 nm in both 9-methylpurine and the purine free base is assigned to several $^1\pi\pi^*$ electronic transitions that overlap strongly in this spectral region (Figure 1). Evidence for this assignment comes from previous experimental[1,3,6] and computational[7,9] works and is reinforced by the present results for both 9-methylpurine and the purine free base (Table 2).

For the purine free base, two pairs of $^1\pi\pi^*$ electronic transitions from both the N7H (S_2 and S_3) and N9H (S_2 and S_4) tautomers contribute to this absorption band to different extents.[7] The lower-energy and more intense transition (~260 nm) is perturbed insignificantly by the solvent used, mainly showing an increase in vibronic resolution when 9-methylpurine is dissolved in cyclohexane (Figure 1b); this is in agreement with previous observations.[1,8] However, as shown in Figure 1b, the higher-energy and less intense electronic transition (~230 to 240 nm) blue-shifts in going from polar protic (buffer) to polar aprotic (acetonitrile) to nonpolar solvents (cyclohexane).

The observed solvatochromic effect is in agreement with the theoretical calculations presented in this work. In view of the oscillator strengths calculated for the $^1\pi\pi^*$ transitions in both tautomers and assuming an equal ratio, the N9H tautomer would contribute more significantly to the low-energy transition at ~260 nm, whereas the N7H tautomer would be mainly responsible for the high-energy transition at ~240 nm. Taking into consideration that

for the N9H tautomer the lowest-energy $^1\pi\pi^*$ state (265 nm) has a dipole moment (3.00 D) comparable to that in the ground state (3.40 D) in the gas phase, the transition at 260 nm should barely be perturbed by the solvent. On the other hand, the calculations show that the dipole moment of the second $^1\pi\pi^*$ state in the N7H tautomer (255 nm) is significantly larger (8.84 D) than the corresponding value in the ground state (5.62 D), suggesting there should be a notable blue-shift in going from polar protic to polar aprotic to nonpolar solvents, as observed in Figure 1a. These results are in agreement with the assignment of purine's spectrum made by Borin et al.[7] except for their prediction that the first $\pi\pi^*$ state of the N7H tautomer contributes more to the main transition at ~260 nm than that of the N9H tautomer. As Figure 1 shows, a larger blue-shift is present in the absorption spectra of the purine free base, as compared to 9-methylpurine, in going from water to acetonitrile in this spectral region (~240 nm). Considering that the change of the dipole in going from the S_0 to the second excited $^1\pi\pi^*$ state is larger in 9-methylpurine than in the N9H tautomer of the purine free base, this shift can only be explained by assuming that the second $^1\pi\pi^*$ state of the N7H tautomer is contributing to the 240 nm absorption shoulder of the purine free base mixture.

A low intensity absorption tail is observed to the red side of the main 260 nm absorption band that shifts further to the red in going from acetonitrile to cyclohexane. This tail is not observed in aqueous buffer solution, suggesting that the electronic transition associated with it shifts to higher energies in this polar protic solvent. These observations are consistent with an electronic transition that is less polar than the ground state and has smaller oscillator strength. Thus, this absorption tail is assigned to an $n\pi^*$ electronic transition that is lower in energy than the lowest two $\pi\pi^*$ electronic transitions in both the purine free base and 9-methylpurine. This assignment is in agreement with previous experiments[1,2,4-6] and calculations.[7,9]

A high-intensity absorption band is also observed at energies above 5.6 eV (< 220 nm in Figure 1). This absorption band red-shifts and decreases in intensity in going from acetonitrile to aqueous solution in both the purine free base and 9-methylpurine, and a further red-shift and decrease in intensity is observed for 9-methylpurine in cyclohexane. This complex solvatochromic behavior suggests that multiple electronic transitions are contributing to this absorption band in different solvents, and from both the N7H and N9H tautomers in the case of the purine free base. This is in agreement with the present and previous calculations,[7] which suggest a superposition of electronic transitions with ππ* and nπ* character above 5.6 eV for both of the N7H and N9H purine tautomers in vacuum.

The results presented in this work show that 9-methylpurine and the purine free base exhibit very small fluorescence yields of ca. 10^{-3}. For 9-methylpurine, the emission maximum blue-shifts and the fluorescence yield decreases approximately fourfold in going from water to cyclohexane. In contrast, the emission maximum in the purine free base does not change appreciably, while its fluorescence yield exhibits approximately a twofold decrease upon going from water to acetonitrile. The comparison of the emission results for 9-methylpurine and the purine free base indicates that both the N7H and N9H purine tautomers contribute to the observed fluorescence. Moreover, based on the theoretical calculations, it is proposed that the observed fluorescence emission originates from the ^{1}nπ* state of both the N7H and N9H purine tautomers and also from the ^{1}nπ* state of 9-methylpurine. This is consistent with the ultrafast decay of the ^{1}ππ* state and the hundreds-of-picoseconds intersystem crossing of the ^{1}nπ* state to the triplet manifold. In fact, the experimental fluorescence maximum for 9-methylpurine of ~370 nm in cyclohexane, as well as the experimental $E_{0,0}$ energy reported in Table S1 of the SI, are in good agreement with the computed vertical (375 nm) and adiabatic (326 nm) emission energies. The S_0 (3.45 D) to S_1 (2.54 D) change in the dipole

moment calculated at the $S_1(n\pi^*)$ minimum geometry, is in line with the blue-shift of the fluorescence maximum experimentally observed when decreasing the polarity of the solvent.

Previous reports have provided conflicting results regarding the fluorescence properties of the purine free base, as remarked recently by Catalán.[8] The results shown in Figure 1 are in good agreement with those reported by Drobnik and Augenstein in 1966.[4] They are also supported by single photon counting experiments,[23] where a long-lived fluorescence lifetime of 5 ns was reported for the purine free base in liquid N_2 at 77K.

3. Broadband Transient Absorption Spectrometer. The experimental setup and data analysis procedure have been described previously.[24-26] Briefly, a Quantronix *Integra-i/e 3.5* Laser generating laser pulses centered at 800 nm with a repetition rate of 1 kHz was used to seed an optical parametric amplifier (OPA, TOPAS, Quantronix / Light Conversion). Laser pulses with a full-width-half-maximum of 100 fs were measured using a *GRENOUILLE* (Model 8-50, Swamp Optics), which is based on the frequency-resolved optical gating (FROG) technique developed by Trebino and coworkers.[27]

The OPA was tuned to the excitation wavelength of 266 nm. Contributions to the excitation beam by other wavelengths or polarizations were removed using a reflective wavelength filter (λ-filter) and a Glan-Taylor prism. The excitation pulses were attenuated to the desired intensity of 1 mJ using a neutral density optical filter in order to minimize cross phase modulation effects and sample degradation.[28,29] Long-lived transient absorption signals originating from hydrated electrons formed by two-photon ionization of the water solvent[30] were effectively minimized under the experimental conditions used in this work. Rotational relaxation effects were removed from the transient absorption signals by randomizing the polarization of the excitation pulses by using a depolarizing plate in the spectrometer.

A broadband transient absorption spectrometer (Helios, Ultrafast Systems, LLC) was used for data acquisition. A continuously moving 2 mm CaF_2 crystal was used for white light continuum generation (WLC) giving access to the spectral range from 350 to 675 nm. The probe pulses were corrected for group velocity dispersion (GVD) using a home-made LabView (National Instruments, Inc.) program as described previously.[24] A pump/probe beam diameter ratio of three was used.

Data analysis was performed using Igor Pro 6.12A software (Wavemetrics, Inc.), as described previously.[31] Nineteen kinetic traces were selected from the multidimensional data set for each compound at selected probe wavelengths and analyzed using a global fitting subroutine set up in the Igor Pro software. The global and target analysis method[32,33] based on a sequential kinetic model[34] was used to obtain the excited-state lifetimes and decay associated spectra. The sequential model rate law was composed of three exponential components.[34] This function was convoluted with a Gaussian-shaped instrument response function with a FWHM of 200 fs. The time constants were linked for all the traces while the amplitudes were left wavelength-dependent. The reported uncertainties for the lifetimes shown in Table 1 are twice the standard deviation (2σ) obtained from the global analysis of at least three independent sets of experiments for each compound.

The absorbance of 9-methylpurine (9MP) and purine (P) solutions were in the range of 0.5 to 1 at the excitation wavelength of 266 nm, which corresponds to millimolar concentrations of the bases. A 2 mm optical path length cell was used in the pump-probe experiments. The samples were continuously stirred using a Teflon-coated stir bar and a magnetic stirrer to avoid re-excitation of the excited volume by successive laser pulses. Solutions were carefully monitored for photodegradation using a spectrophotometer (Cary 100, Varian, Inc.) and were replaced with fresh solutions before a 10 % decrease in steady-state absorbance at the excitation wavelength was observed.

4. Methodology used for Estimating $E_{0,0}$ and Fluorescence Quantum Yields. Steady-state absorption and emission spectra were measured at room temperature using Cary 100 Bio and Cary Eclipse spectrophotometers (Varian, Inc.), respectively. Background corrections were performed by subtracting a solvent-only scan under the same experimental conditions. Fluorescence spectra were taken at high PMT voltage with slit-widths of 5 nm and averaging times of 2 s. All solutions were made with an optical density of ~0.2 at the excitation wavelength of 267 nm.

Calculations of fluorescence quantum yield were performed using Equation 1:

$$\Phi_f^{un} = \frac{n_{un}^2 I_{un} OD_S}{n_S^2 I_S OD_{un}} \Phi_f^S \qquad (1)$$

where Φ_f represents the fluorescence quantum yield, *OD* is the optical density (i.e. steady-state absorption at the excitation wavelength), *I* is the integrated area under the emission spectrum, and *n* is the refractive index of the respective solvent.[35] The subscripts *s* and *un* stand for the fluorescence standard and unknown, respectively. When calculating quantum yields, it is common to use the same solvent for the standard and unknown; thus the *n* terms are made equal by assuming the low concentrations used do not change the solvent refractive index. While this was done for the solutions in PBS, using the reported Φ_f^s for Tryptophan (Trp) of 0.13 ± 0.1,[35] the necessary standard Φ_f of Trp in acetonitrile and cyclohexane could not be found; therefore, the refractive indices of these solvents were used to calculate the respective Φ_{Fl} of purine free base and 9-methylpurine.

The transition energy between the lowest vibrational levels of the ground state and $^1\pi\pi^*$ state were determined for the purine free base and 9-methylpurine from the crossing point of their absorption and emission spectra (Table S1 and Figures S1 and S2). Absorption spectra were used rather than excitation spectra for these $E_{0,0}$ determinations due to the

difficulty of obtaining accurate excitation spectra at wavelengths shorter than 300 nm, especially working with compounds having low fluorescence quantum yields.[36] Emission spectra were obtained on a wavelength (nm) scale using a constant band-pass setting; therefore, following their conversion to wavenumbers (cm^{-1}), the emission intensities needed to be corrected by multiplying each intensity by its collection wavelength squared (λ^2).[35]

Table S1. Fluorescence quantum yields and zero-zero energies for purine free base (P) and 9-methylpurine (9MP) in aqueous buffer solution (PBS, pH 7), acetonitrile (ACN), and cyclohexane (CHX)

Base	Solvent	$\Phi_{Fl} \times 10^{-3}$ [a]	$E_{0,0}$ (cm^{-1})	$E_{0,0}$ (eV)
P	PBS	4.4 ± 0.3	32,472	4.03
P	ACN	2.0 ± 0.2	32,126	3.98
9MP	PBS	4.0 ± 0.3	32,124	3.98
9MP	ACN	2.4 ± 0.2	31,929	3.96
9MP	CHX	1.2 ± 0.2	nd	nd

[a] reported errors are equal to one standard deviation of three independent measurements; nd = not determined.

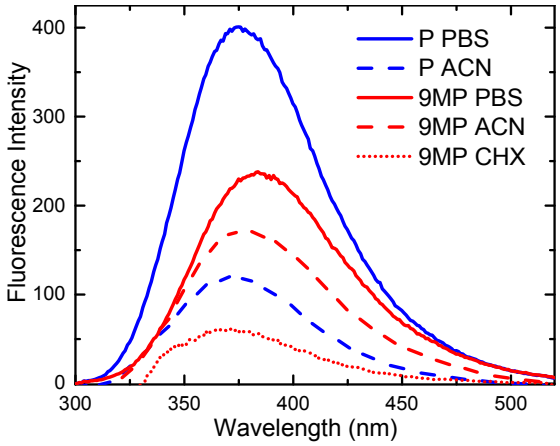

Figure S1. Emission spectra of purine free base (P) and 9-methylpurine (9MP) in aqueous buffer solution, pH 7 (PBS), acetonitrile (ACN), and cyclohexane (CHX) recorded in back-to-back with identical optical densities at the excitation wavelength (OD = 0.20 at 267 nm).

DOI: 10.1021/ja512536c

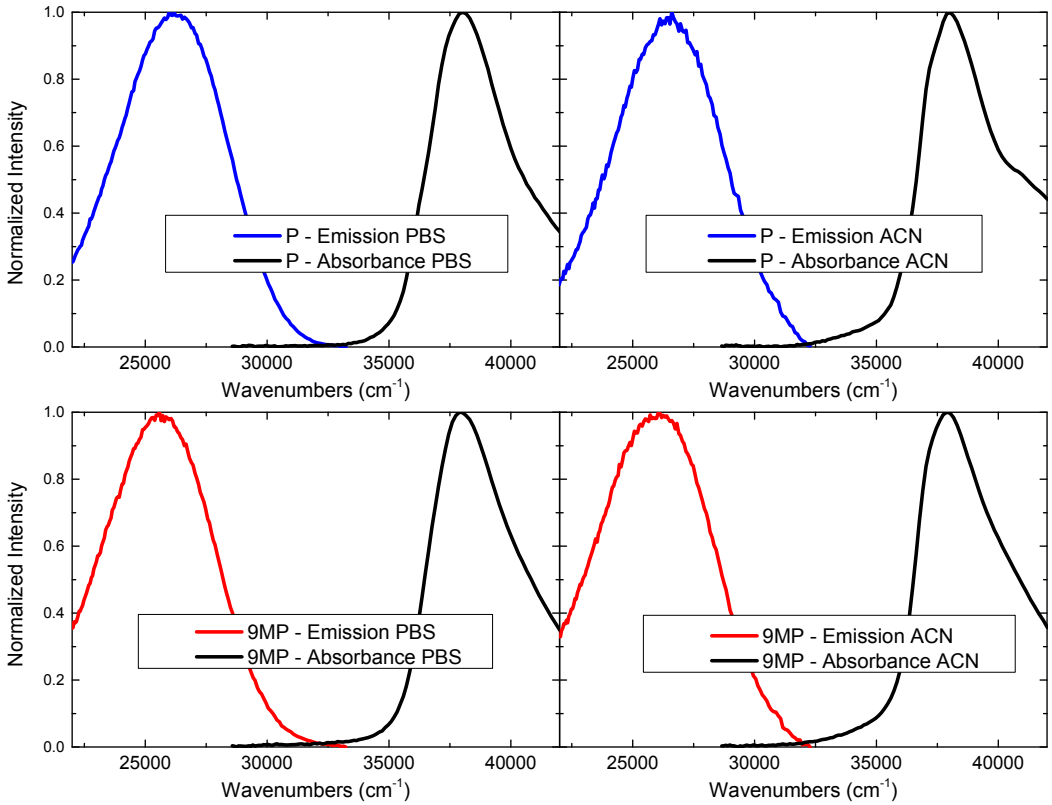

Figure S2. Absorption and emission spectra used to calculate the fluorescence quantum yields and zero-zero energies of the purine free base (P) and 9-methylpurine (9MP).

DOI: 10.1021/ja512536c
J. Am. Chem. Soc. **2015**, S9

5. Contour plots of the multidimensional transient absorption data and the non-normalized spectra of 9-methylpurine in acetonitrile.

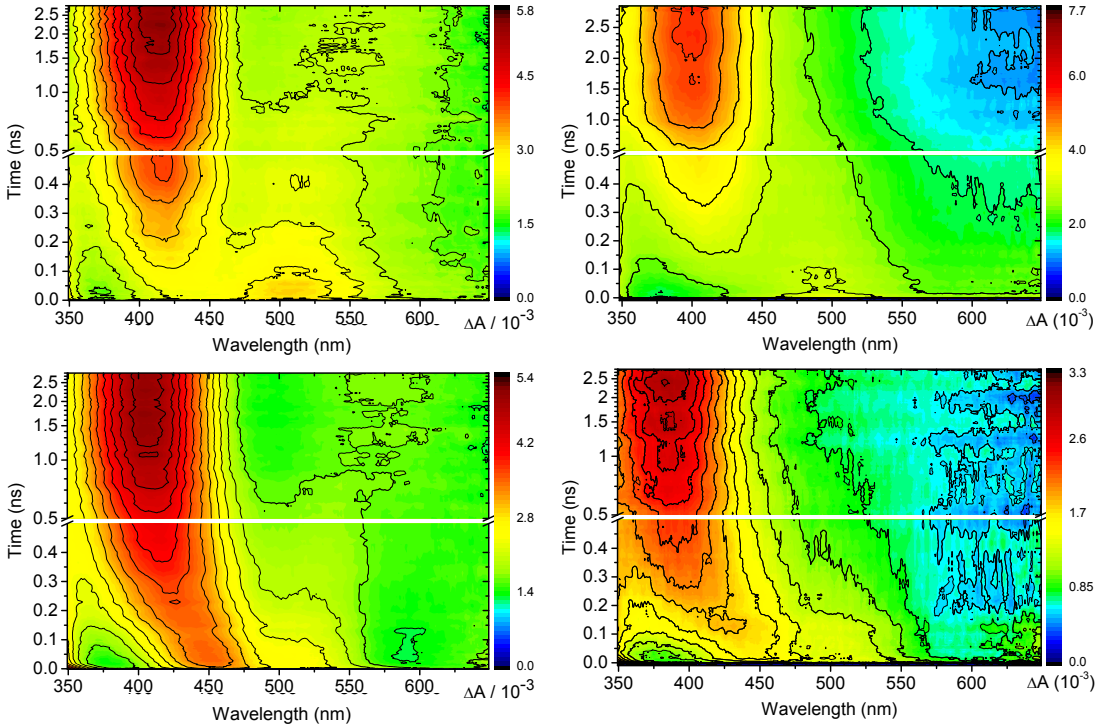

Figure S3. Contour plot of the transient absorption spectra of 9MP (left) and P (right) in aqueous buffer solution pH 7 (top) and acetonitrile (bottom) after 266 nm excitation.

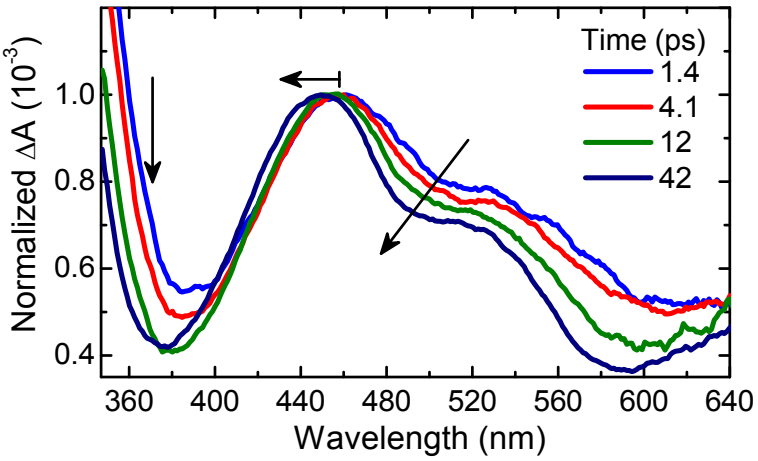

Figure S4. Normalized transient absorption spectra obtained for 9-methylpurine in acetonitrile shown in the left-middle panel of Figure 2. This normalization highlights the blue shifting and narrowing of the absorption band during the reported time delays which are characteristic of vibrational cooling dynamics.

DOI: 10.1021/ja512536c
J. Am. Chem. Soc. **2015**, S10

II. COMPUTATIONAL METHODS & SUPPORTING RESULTS

1. Density Functional Calculations. The DFT and TD-DFT calculations presented in Table S2 and Figure S5 were performed using the Gaussian 03 suite of programs.[37] Ground-state optimizations were performed using the parameter-free PBE0 functional.[38] Optimized ground-state geometries were calculated without any geometrical restriction. The gas-phase optimized geometries for 9MP and 9MP$(H_2O)_3$ complex were confirmed to be local minima on the ground-state potential energy surface through vibrational frequency analysis at the PBE0/6-31G level of theory. The ground-state geometry of 9MP was further optimized in vacuum at the PBE0/6-31+G(d,p) level of theory. Excited-state calculations were performed using the PBE0 functional. The PBE0 functional provides accurate excited-state energies,[39,40] singlet-triplet energy gaps,[41] excited-state ordering,[22,42] and ground-state absorption spectra,[39] particularly when solvent effects are taken into account.[39,42,43] Solvent effects on the excited-state vertical energies were modeled by performing self-consistent reaction field (SCRF) calculations using the polarizable continuum model (PCM)[44] with the integral equation formalism (SCRF=IEFPCM).[45] Additional calculations were performed that include explicit solute-solvent interactions when modeling the water solvent. In this case, vertical excitation energies for the 9MP$(H_2O)_3$ complex also include bulk solvent effects. Basis set superposition errors were not considered as they are not expected to significantly influence the semi-quantitative results obtained in this "super-molecule" approach. Excited-state energies are presented at the TD-PBE0/IEFPCM/6-311++G(d,p) level of theory throughout the calculations presented in Table S2 and Figure S5.

DOI: 10.1021/ja512536c

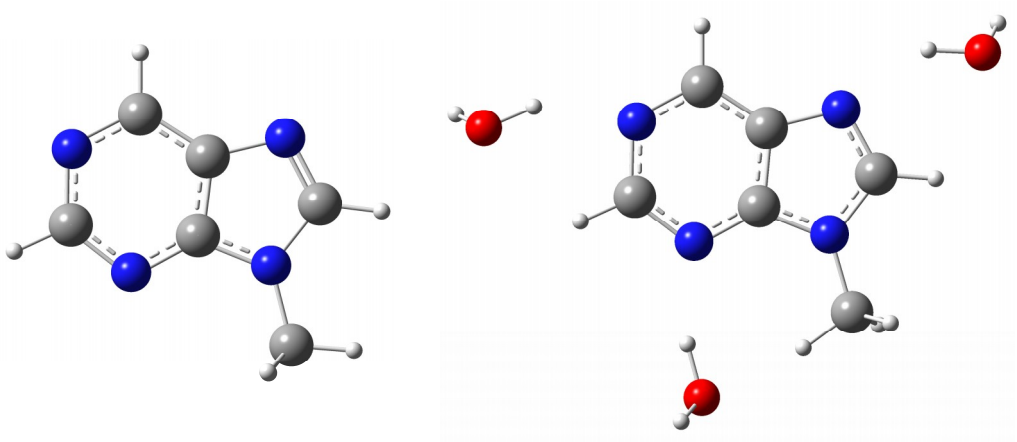

Figure S5. Gas-phase structures of the 9MP (left) and 9MP$(H_2O)_3$ complex (right) optimized at the PBE0 level of theory using the 6-31+G(d,p) and 6-31G basis sets, respectively.

Table S2. TD-DFT/PBE0/IEF-PCM/6-311++G(d,p)//B3LYP/6-31+G(d,p) vertical singlet and triplet excitation energies for 9-methylpurine (9PM) and the complex between 9-methylpurine and three water molecules (9MP$(H_2O)_3$))

State	9MP **Gas Phase**	9MP **Cyclohexane**	9MP **Chloroform**	9MP **ACN**	9MP **Water**	9MP$(H_2O)_3$ **Gas Phase**	9MP$(H_2O)_3$ **Water**[a]
$T_1(\pi\pi^*)$	3.42 eV 362.46 nm	3.43 eV 360.98 nm	3.44 eV 359.82 nm	3.45 eV 359.00 nm	3.45 eV 359.00 nm	3.43 eV 361.36 nm	3.47 eV 357.61 nm
$T_2(n\pi^*)$	3.93 eV 315.78 nm	4.00 eV 310.08 nm	4.06 eV 305.14 nm	4.12 eV 301.01 nm	4.13 eV 300.35 nm	4.27 eV 290.09 nm	4.30 eV 288.33 nm
$T_3(\pi\pi^*)$	4.38 eV 283.23 nm	4.37 eV 283.71 nm	4.36 eV 284.20 nm	4.36 eV 284.68 nm	4.35 eV 284.76 nm	4.33 eV 286.51 nm	4.37 eV 283.51 nm
$T_4(n\pi^*)$	4.71 eV 263.20 nm	4.79 eV 259.06 nm	4.85 eV 255.50 nm	4.91 eV 252.53 nm	4.92 eV 252.12 nm	5.09 eV 243.74 nm	5.13 eV 241.85 nm
$T_5(\pi\pi^*)$	4.73 eV 262.36 nm	4.72 eV 262.90 nm	4.71 eV 263.44 nm	4.70 eV 263.94 nm	4.70 eV 264.05 nm	4.68 eV 265.14 nm	4.72 eV 262.68 nm
$S_1(n\pi^*)$	4.32 eV 287.10 nm f=0.0018	4.39 eV 282.54 nm f=0.0023	4.45 eV 278.33 nm f=0.0024	4.51 eV 274.74 nm f=0.0024	4.52 eV 274.23 nm f=0.0024	4.67 eV 266.32 nm f=0.0018	4.68 eV 265.17 nm f=0.0018
$S_2(\pi\pi^*)$	5.15 eV 240.81 nm f=0.1255	5.12 eV 242.12 nm f=0.1801	5.11 eV 242.46 nm f=0.1692	5.12 eV 242.33 nm f=0.1440	5.12 eV 242.38 nm f=0.1414	5.08 eV 243.98 nm f=0.1230	5.11 eV 242.48 nm f=0.1269
$S_3(\pi\pi^*)$	5.30 eV[b] 233.83 nm f=0.0254	5.23 eV 236.93 nm f=0.0393	5.27 eV 235.42 nm f=0.0478	5.26 eV 235.70 nm f=0.0539	5.26 eV 235.79 nm f=0.0549	5.23 eV 237.11 nm f=0.0749	5.26 eV 235.51 nm f=0.0775
$\Delta E(S_2 - S_1)$	0.83 (6,694.4 cm^{-1})	0.73 (5,887.8 cm^{-1})	0.66 (5,323.3 cm^{-1})	0.61 (4,9120.0 cm^{-1})	0.60 (4,839.3 cm^{-1})	0.41 (3,306.9 cm^{-1})	0.43 (3,468.2 cm^{-1})
$\Delta E(S_1 - T_1)$	0.90 (7,259.0 cm^{-1})	0.96 (7,742.9 cm^{-1})	1.01 (8,146.2 cm^{-1})	1.06 (8,549.5 cm^{-1})	1.07 (8,630.1 cm^{-1})	1.24 (10,001.3 cm^{-1})	1.21 (9,759.3 cm^{-1})
$\Delta E(S_1 - T_3)$	-0.06	0.02	0.09	0.15	0.17	0.34	0.31

[a] ground state optimized at PBE0/6-31+G(d,p); [b] S_4 in the gas phase. S_3 has mostly nπ* character (5.18 eV, 0.0014) in the gas phase.

DOI: 10.1021/ja512536c
J. Am. Chem. Soc. **2015**, S12

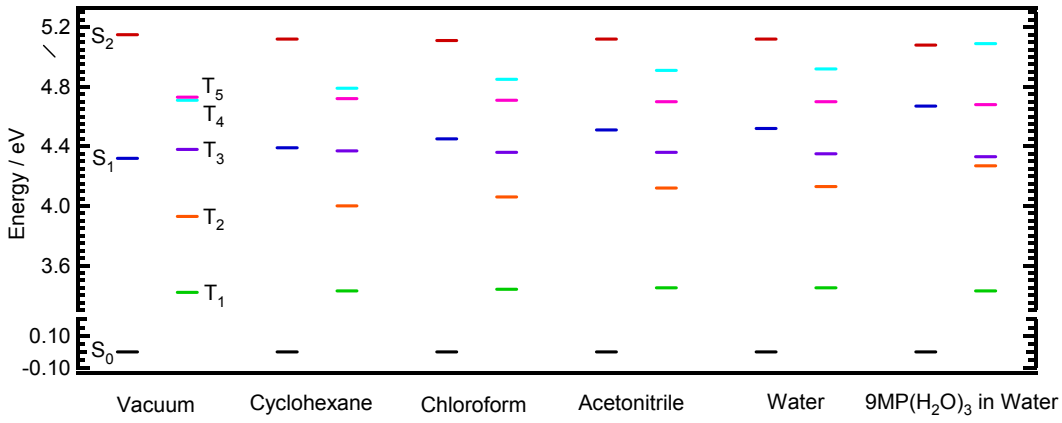

Figure S6. Energy diagrams for the vertical excitation energies of 9MP as a function of solvent and 9MP$(H_2O)_3$ complex in water relative to the ground state calculated at the TD-PBE0/IEFPCM/6-311++G(d,p) level of theory. The excited-states are color-coded relative to the state assignments in vacuum.

2. CASSCF and CASPT2 Calculations. The ground-state absorption spectra of N9H purine and 9-methylpurine were calculated at the equilibrium geometries optimized with the complete active space self-consistent field (CASSCF) method[46] and the ANO-L basis set contracted as C,N [4s3p2d]/H[3s2p],[47] using no symmetry constraints. The active space employed comprises 16 electrons distributed in 12 orbitals, and includes 3 lone-pairs sitting on the nitrogen atoms 1, 3 and 7 (Scheme 1) and the complete set of π and π* orbitals (5 bonding and 4 anti-bonding), see Figure S7. The CASSCF calculations were performed state averaged (SA) over 10 singlet and 10 triplet roots. Dynamic correlation was incorporated using multi-state second order perturbation theory, MS-CASPT2,[48,49] on reference SA-CASSCF wavefunctions. An imaginary level shift parameter[50] of 0.3 au was added to the zero order Hamiltonian to prevent the appearance of intruder states and the IPEA shift[51] was set to zero. The effect in the absorption spectra of N9H purine and 9-methylpurine of different solvent environments was simulated using the PCM model as implemented in

DOI: 10.1021/ja512536c

MOLCAS. A comparison of the different simulated absorption spectra with the experimental ones is provided in Fig. S8.

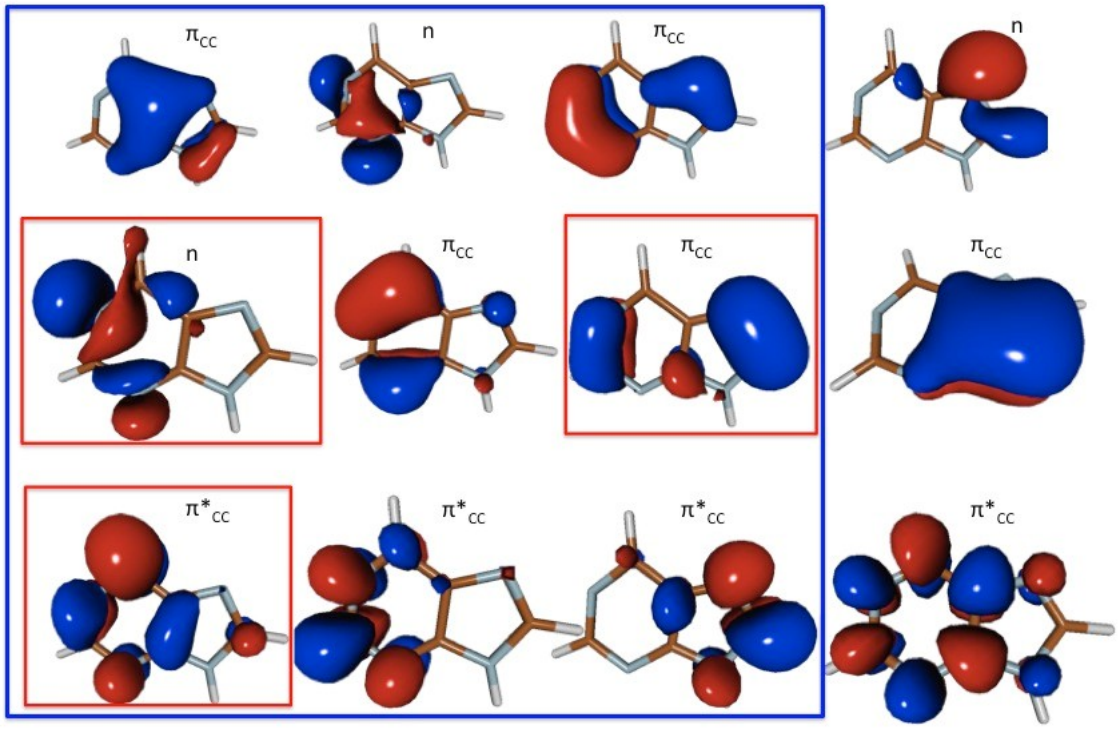

Figure S7. Orbitals involved in the (16,12) active space optimized for the ground state of P. Framed in blue the (12,9) active space used during the dynamics simulations and framed in red the orbitals involved in the $S_1(n\pi^*)$ and S_2 ($\pi\pi^*$) excitations discussed throughout the manuscript.

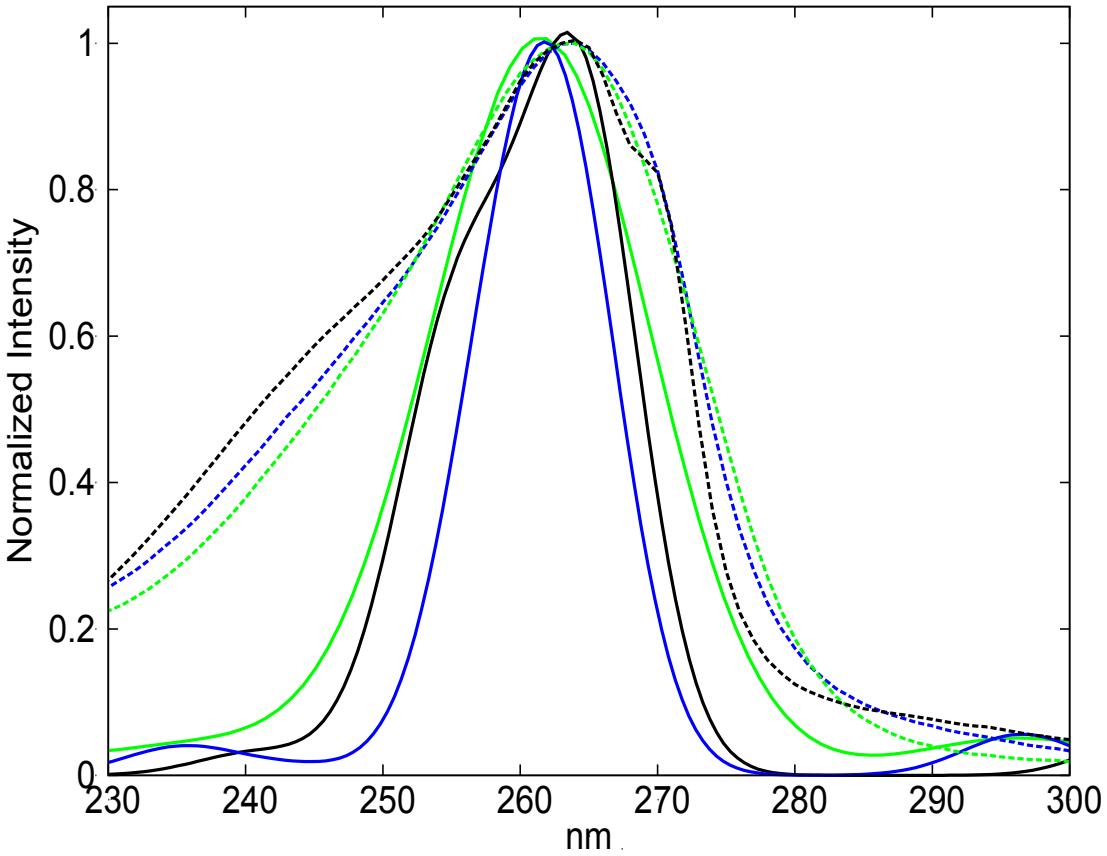

Figure S8. Simulated theoretical MS-CASPT2 (solid lines) and experimental (dashed lines) absorption spectra in gas phase (black, cyclohexane was used for the experimental case), water (green), and acetonitrile (blue), using a width at half maximum of 5 nm.

DOI: 10.1021/ja512536c
J. Am. Chem. Soc. **2015**, S15

Transient absorption spectra in Figures 8 and S9 were simulated at the corresponding ground or excited state optimized geometries using the MS-CASPT2//SA-CASSCF (16,12)/ANO-L protocol, and employing the necessary number of roots to cover the experimental absorption range. The line broadening method, which assigns a Gaussian to each of the calculated absorptions, was employed for a better comparison with the experiment. A detailed procedure for weighting the simulated transient absorption spectra and their utility in clarifying the excited-state dynamics are given below (Figures S9 and S10).

Minimum energy paths (MEPs) in Figures S11 to S16 were computed following the intrinsic reaction coordinate (IRC) algorithm to locate energy-accessible stationary points (Table S4 and Figure S17). These calculations were performed using the CASSCF/ANO-S protocol (contraction scheme: C,N[3s2p1d]/H[2s1p]) with the same (16,12) active space employed for the optimization of the ground state (see Figure S7) and the number of roots necessary. The same protocol was employed for the optimization of the stationary points found along the deactivation pathway, while the location of singlet-singlet and singlet-triplet minimum energy crossing points was done with the Pople basis set 6-31G*. Final energies for all the minima and conical intersections along the relaxation pathways were computed at MS-CASPT2//SA-CASSCF(16,12)/ANO-L over 3 singlet or 3 triplet roots. Reference CASSCF(16,12) wavefunctions were obtained through state-average calculations using 3 singlet or 3 triplet roots, respectively.

In general, the CASSCF and CASPT2 methods find different qualitatively and/or quantitatively descriptions of the potential energy surfaces in the vicinity of the $^1(\pi\pi^*)$ minimum and at the degeneracy regions between different electronic states of the same or different multiplicity. The inclusion of dynamical correlation typically increases the energy gap between the states involved in the surface crossings. In these cases, singlet/singlet and singlet/triplet crossings were re-optimized with the help of the gradient difference vector,

until an energy difference smaller than 0.2 eV between the two intersecting states was reached at MS-CASPT2 level of theory. For the correct description of the early stages of the deactivation mechanism, we optimized the $^1(\pi\pi^*)$ minimum using CASPT2 gradients and the smaller active space (6,5).

The probability of intersystem crossing along the MEP was estimated by calculating spin-orbit coupling terms at critical points of the potential energy surfaces, namely at the Franck-Condon geometry, singlet minima and singlet/triplet minimum energy crossing points. These calculations were performed using SA-CASSCF(16,12)/ANO-RCC wavefunctions including 3 singlet and 3 triplet states.

Vertical spectra, minimum energy paths, geometry optimizations, final energies, and spin-orbit couplings were obtained with the MOLCAS-76 program.[52] The optimization of singlet-singlet and singlet-triplet minimum energy crossing points was done with MOLPRO 2009.[53]

3. Comparison of Simulated and Experimental Transient Absorption Spectra. Experimental spectra shown in Figure 8 were extracted from the transient data for 9-methylpurine in acetonitrile. The spectra were chosen at time delays where the signals reached a maximum intensity before beginning to decay. As mentioned above, the absorption spectrum of each individual excited-state was simulated by Gaussian broadening (50 nm width-at-half maximum) of the calculated transition oscillator strengths (Figure S9). At each of the four chosen time delays, the spectrum was simulated by linear combination of multiple computed excited-state absorption spectra. The excited-state spectra included in each linear combination were selected based on the time delay and the predicted major relaxation pathway from the static and dynamics simulations. The contribution of each excited-state absorption to the linear combination was weighted until the simulated spectra best matched the experimental spectra as quantitatively as possible. The coefficient required for each

excited-state absorption in the linear combination, which is reported in the following paragraph, was then used to support the decay mechanism of the purine free base and 9-methylpurine.

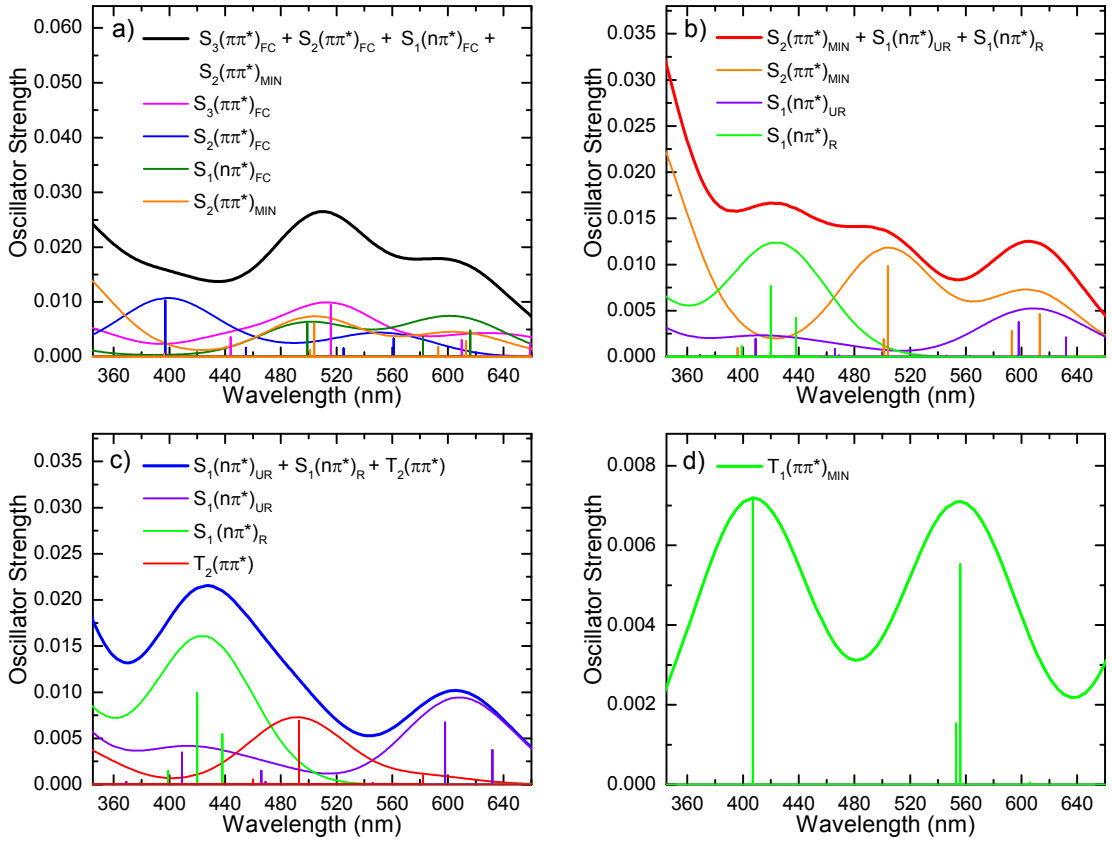

Figure S9. Individual components and the corresponding simulated transient absorption spectra shown in Figure 8. The absorption spectra of the individual excited states were computed for 9-methylpurine in vacuum using MS-CASPT2. The spectrum of each excited state was scaled so that their linear combination best matched the experimental spectrum at the given time delay. The oscillator strengths shown here are those that have been scaled to produce the linear combinations (unscaled oscillator strengths given in Table S7). The coefficients used for each linear combination are given in the text below and in the caption of Figure 8. The experimental spectra at time delays of (a) 0.03 ps, (b) 1.4 ps, (c) 42 ps, and (d) 2600 ps were used to match with these simulations.

Based on these simulated spectra, at a delay of 0.03 ps (Figure S9a) we have population in the $S_3(\pi\pi^*)_{FC}$ (0.25), $S_2(\pi\pi^*)_{FC}$ (0.25), and $S_1(n\pi^*)_{FC}$ (0.25) states at the Franck-Condon region, as well as population already at the $S_2(\pi\pi^*)_{MIN}$ (0.25) near the conical

intersection with the S_1 state, $(S_2(\pi\pi^*)/S_1(n\pi^*))_{CI}$. This lines up favorably with percentages calculated from semiclassical dynamics simulations for the population of each state upon 266 nm excitation, 7% to S_3, 80% to S_2, and 13% to S_1 (Figure 6); if we assume that some decay from the $S_2(\pi\pi^*)_{FC}$ to the $(S_2(\pi\pi^*)/S_1(n\pi^*))_{CI}$ occurs faster than our time resolution (supported by the steep slope of the PES between these two regions, see Figure 7).

At a time delay of about 1.4 ps (Figure S9b), the major decay is internal conversion to populate three major areas of the potential energy surfaces: the $S_2(\pi\pi^*)_{MIN}$, the vibrationally-hot (unrelaxed) S_1 state, $S_1(n\pi^*)_{UR}$, and the relaxed S_1, $S_1(n\pi^*)_R$ with an ultrafast lifetime of 0.15 ± 0.05 ps. The populations estimated from the simulated spectrum at 1.4 ps is as follows. The $S_3(\pi\pi^*)_{FC}$ and $S_2(\pi\pi^*)_{FC}$ decay to populate the $S_2(\pi\pi^*)_{MIN}$ (0.42), the population that was already at $S_2(\pi\pi^*)_{MIN}$ near the $(S_2(\pi\pi^*)/S_1(n\pi^*))_{CI}$ internally converts to populate $S_1(n\pi^*)_{UR}$ (0.15), and the population that was initially excited to the $S_1(n\pi^*)_{FC}$ relaxes to $S_1(n\pi^*)_R$ (0.43). The band at ~520 nm is assigned to the $S_2(\pi\pi^*)_{MIN}$ absorption because of the prominent and simultaneous decay of the band at ~350 nm where the $S_2(\pi\pi^*)_{MIN}$ has a very high relative oscillator strength (see Figures 2 and 8 and Table S7 for clarification of this fact).

The major decay mechanism with a tens of picoseconds lifetime (maximum signal at 42 ps, Figure S9c) is vibrational cooling. The population that was left at the $(S_2(\pi\pi^*)/S_1(n\pi^*))_{CI}$ internally converts to populate $S_1(n\pi^*)_{UR}$ (0.36). The population that was already at $S_1(n\pi^*)_{UR}$ vibrationally cools to populate $S_1(n\pi^*)_R$ (0.52). A small fraction of the population that was already at $S_1(n\pi^*)_R$ intersystem crosses to populate the $T_2(\pi\pi^*)$ state (0.12). This small amount of population in the $T_2(\pi\pi^*)$ state is in good agreement with the fraction of singlet population that should have intersystem crossed to the triplet manifold with a lifetime of 350 ± 10 ps, as can be observed based on exponential modeling of this population transfer event (Figure S10).

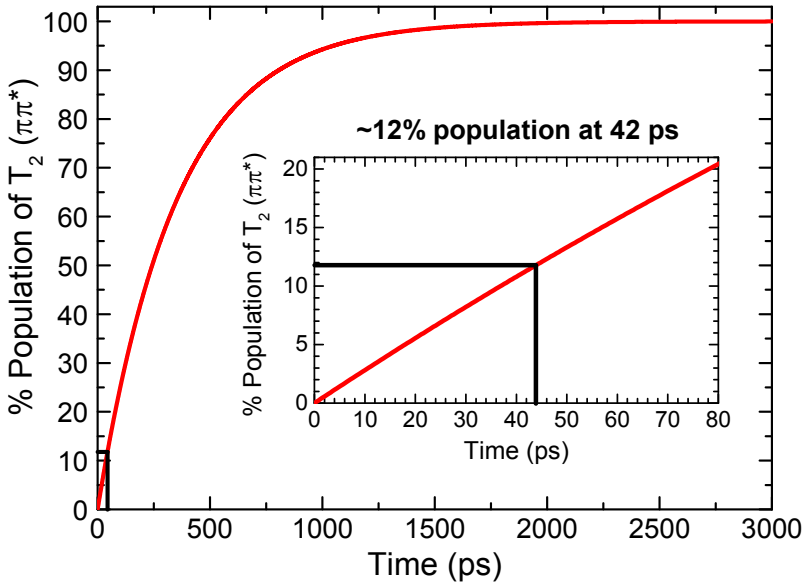

Figure S10. Modeling the exponential growth of population in the $T_2(\pi\pi^*)$ state of 9-methylpurine in acetonitrile based on the 350 ± 10 ps intersystem crossing lifetime, which was determined from a global analysis of experimental transient data. Modeling was performed in order to rationalize the small fraction of $T_2(\pi\pi^*)$ state absorption required to simulate the transient absorption spectrum at 42 ps.

Finally, the excited-state population fully reaches the $T_1(\pi\pi^*)$ state minimum within 2600 ps (Figure S9d) through intersystem crossing from the $S_1(n\pi^*)_R$ and subsequent conformational relaxation from $T_2(\pi\pi^*)$ area of the $^3\pi\pi^*$ potential energy surface (see Figure 7). Apparently, conformational relaxation in the $^3\pi\pi^*$ potential energy surface (i.e., $T_2(\pi\pi^*) \rightarrow T_1(\pi\pi^*)$) occurs on an ultrafast time scale such that there is no further buildup of the $T_2(\pi\pi^*)$ population than the population already observed at 42 ps. This is consistent with the dynamics simulations where no appreciable population in the $T_2(\pi\pi^*)$ is observed (Figure S18, top panel).

4. Dynamical Calculations and Initial Conditions. The absorption spectrum of Figure 6 has been calculated using a Wigner distribution encompassing 1000 geometries, as described in Refs. 54 and 55 with frequencies obtained using MP2/def2-svp.[56] The spectrum is composed

as the sum of Gaussian functions assigned to all transitions of each of the 1000 geometries, computed at the SA-CASSCF(12,9)/def2-svp level of theory, averaged over 5 singlet states.

A sample of 94 initial conditions is used to run ab initio molecular dynamics during 1 ps. The distribution into the initial electronic states is selected according to the computed excitation energies and oscillator strengths.[57,58] In the same way as the experimental excitation window is centered at the maximum of the spectrum, the simulated excitation window was centered at the theoretical absorption maximum of 5.7 eV. The width of the theoretical excitation window was chosen as 0.5 eV, which lead to 12 trajectories starting in the S_1, 75 starting in the S_2, and 7 starting in the S_3. Trajectories were terminated earlier than 1 ps if relaxation to the ground state or to the T_1 state occurred. The employed time step in the nuclear dynamics was 0.5 fs while the time step for integration of the time-dependent Schrödinger equation was 0.02 fs. The energies, gradients, non-adiabatic couplings, and spin-orbit couplings were calculated on-the-fly using SA-CASSCF(12,9)/def2-svp, state-averaged over 4 singlet and 6 triplet states. The dynamical simulations were done with the program SHARC.[59,60]

Singlet-singlet, triplet-triplet and singlet-triplet hopping geometries were used as starting points for optimizations of minimum energy crossings at SA-CASSCF(12,9)/6-31G* level of theory. These optimizations, as well as the on-the-fly quantum calculations have been carried out using the MOLPRO 2012 program package.[61]

The populations plotted in Figure S18 are adiabatic energies (S_0, S_1, S_2 and so on). Since in the dynamics the planar symmetry of the chromophore is generally lost due to the general motion of the molecule, nπ* and ππ* states mix, e.g., at some geometries S_1 might be primarily nπ* and at other geometries ππ*. Hence, it is difficult for the dynamics to disentangle the populations in terms of these state characters. However, in the case of the purine, the S_1 state mostly correlates to nπ* and the S_2 state to the ππ* character. The triplet

characters were checked for all relevant trajectories at 1 ps, and T_1 state has ππ* character in all cases.

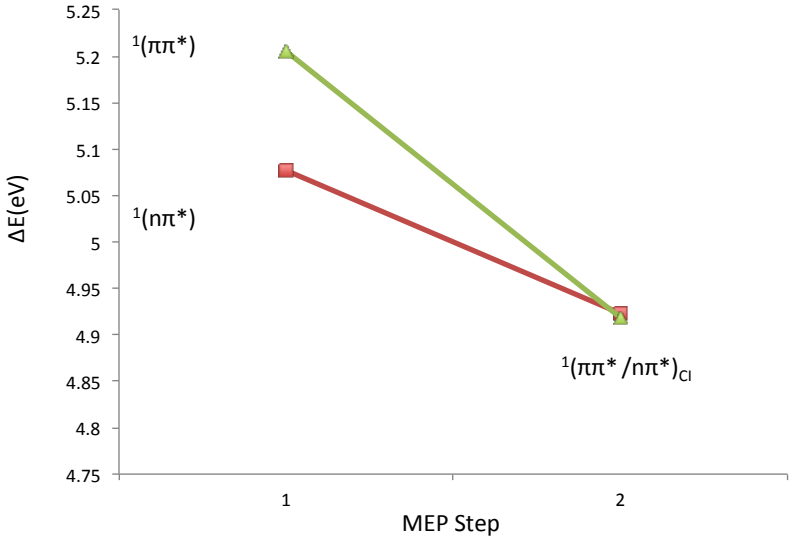

Figure S11. CASSCF minimum energy paths from the Franck-Condon region following the S_3 gradient.

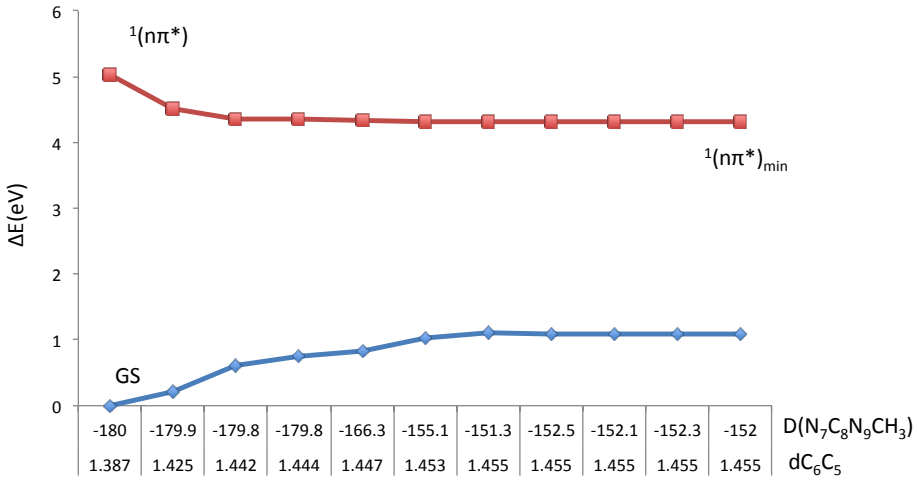

Figure S12. CASSCF minimum energy paths from the Franck-Condon region following the S_2 gradient. Distances are reported in Angstroms and angles in degrees.

DOI: 10.1021/ja512536c
J. Am. Chem. Soc. **2015**, S22

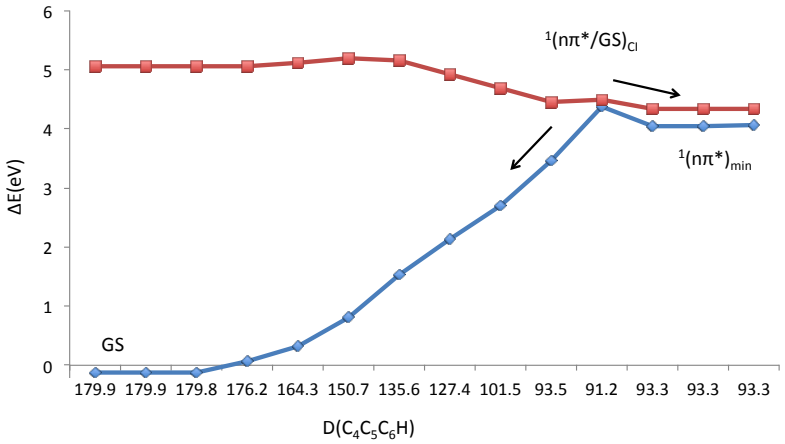

Figure S13. CASSCF minimum energy paths from the $S_1(n\pi^*)/S_0$ conical intersection following the S_1 and S_0 gradients. Angles are reported in degrees.

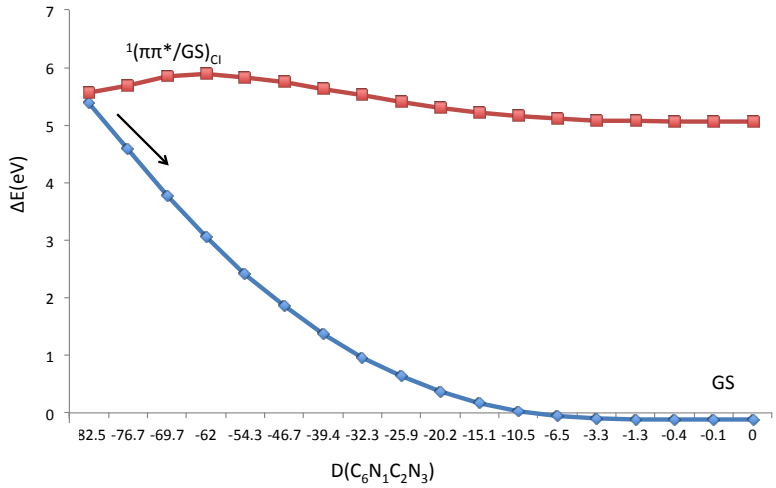

Figure S14. CASSCF minimum energy paths from the $S_1(n\pi^*)/S_0$ conical intersection following the S_0 gradient. Angles are reported in degrees.

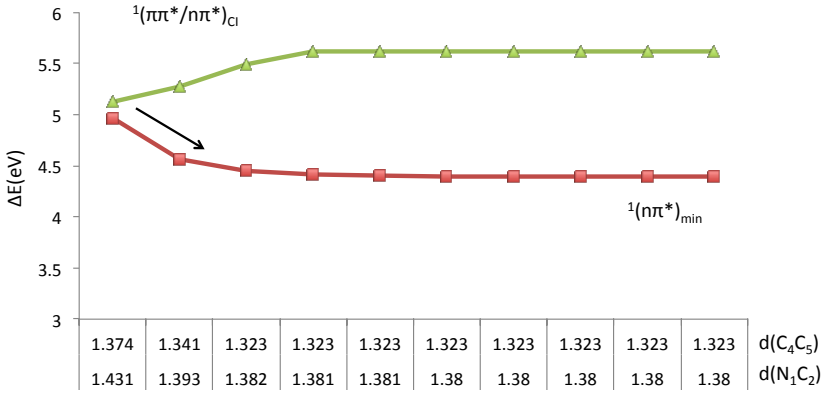

Figure S15. CASSCF minimum energy paths from the $S_2(\pi\pi^*)/S_1(n\pi^*)$ conical intersection following the S_1 gradient. Distances are reported in Angstroms.

DOI: 10.1021/ja512536c

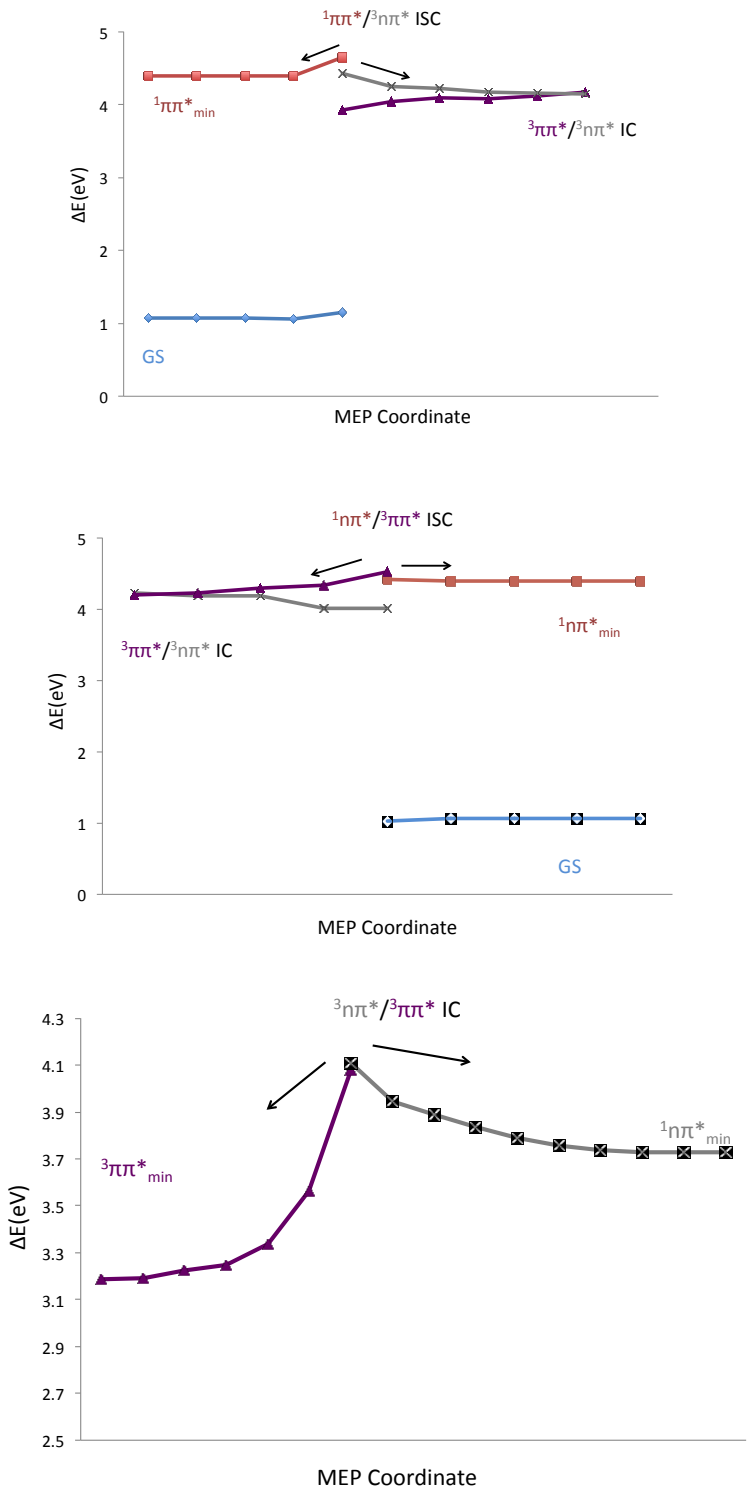

Figure S16. CASSCF minimum energy paths from $S_2(\pi\pi^*)/T_2(n\pi^*)$ and $S_1(n\pi^*)/T_1(\pi\pi^*)$ intersystem crossings and $T_2(n\pi^*)/T_1(\pi\pi^*)$ conical intersection following the indicated gradients.

DOI: 10.1021/ja512536c
J. Am. Chem. Soc. **2015**, S24

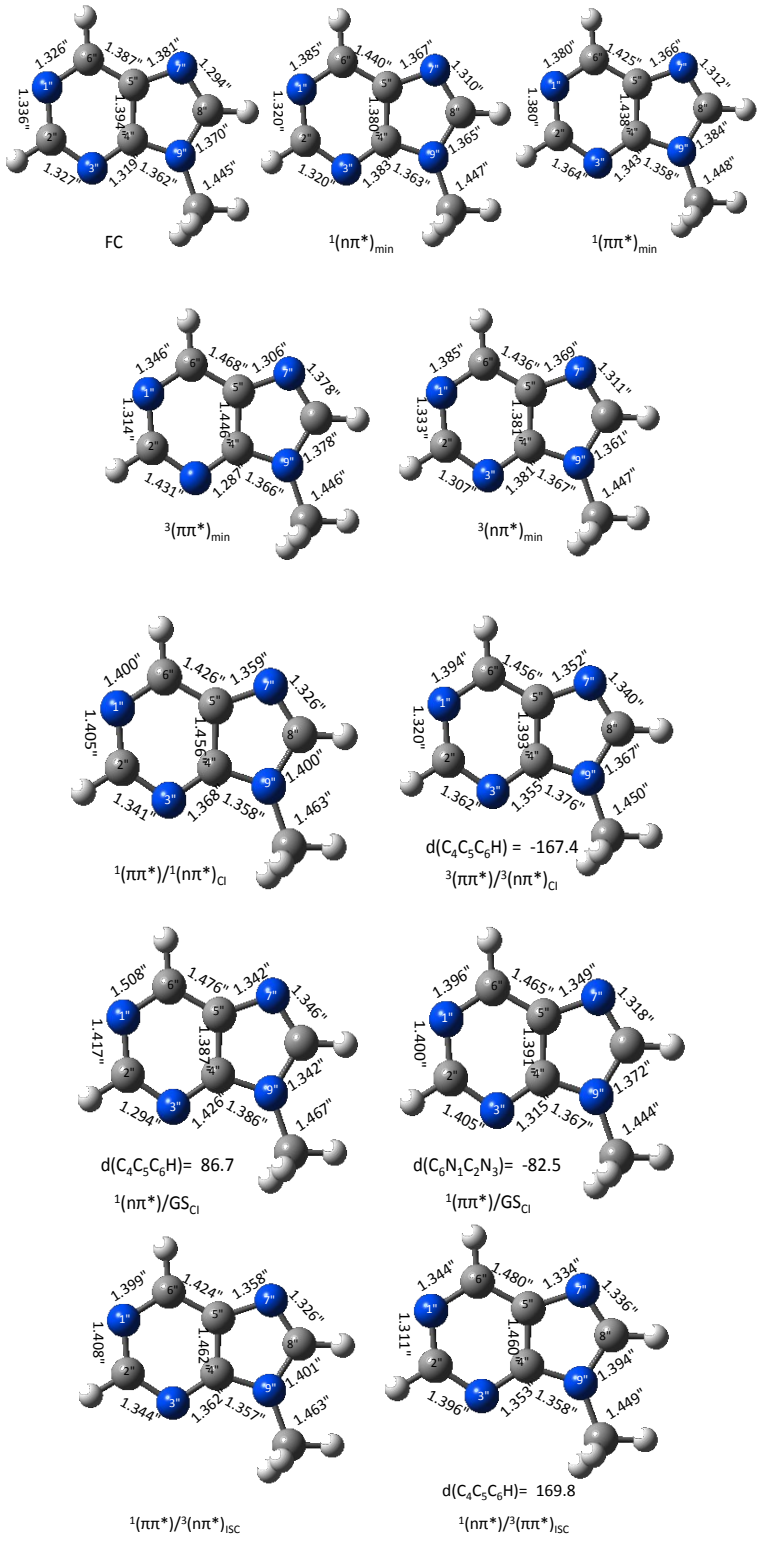

Figure S17. CASSCF optimized conical intersections. Relevant distances are reported in Angstroms and dihedral angles in degrees.

DOI: 10.1021/ja512536c
J. Am. Chem. Soc. **2015**, S25

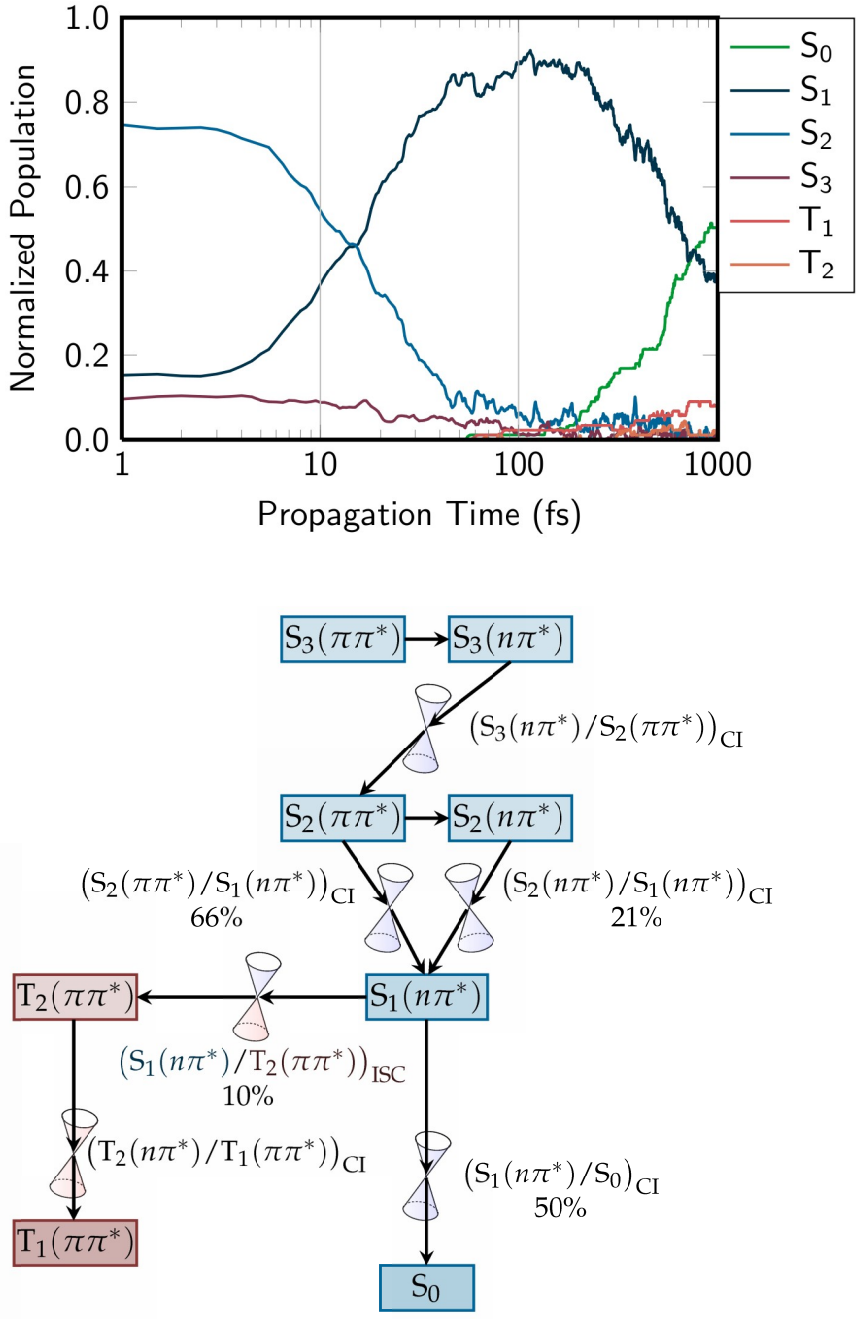

Figure S18. Top panel: Semi-logarithmic plot showing the state populations obtained by ab initio molecular dynamics simulations. Bottom panel: Deactivation mechanism for the N9H tautomer of the purine free base obtained from ab initio molecular dynamics. CI and ISC stand for conical intersection and intersystem crossing, respectively.

DOI: 10.1021/ja512536c
J. Am. Chem. Soc. **2015**, S26

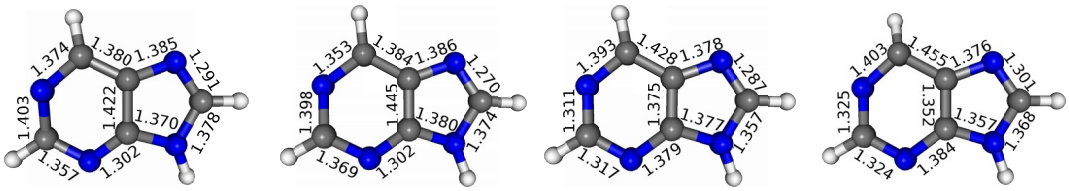

$d(C_6N_1C_2N_3)$=43.47

S_2/S_1 $(n\pi^*)^1/(n\pi^*)^1$ S_3/S_2 $(n\pi^*)^1/(\pi\pi^*)^1$ S_1/T_2 $(n\pi^*)^1/(\pi\pi^*)^3$ T_2/T_1 $(\pi\pi^*)^3/(n\pi^*)^3$

Figure S19. Conical intersections optimized starting from hopping geometries of the dynamical simulations. Relevant distances are reported in Angstroms and dihedral angles in degrees.

Table S3. Singlet vertical absorption energies (in eV) calculated under Cs symmetry constraints of purine free base at CASSCF(16,12)/ANO-L and MS-CASPT2//CASSCF levels of theory.

State	ΔE (ev)	ΔE (ev)[9]	ΔE (ev)[7]	Exp[1,3,8,62]
2A''	4.88	4.801	4.66	4.7
3A''	5.42	5.268	5.09	5.2
4A''	6.38	6.394	6.28	

Tables S4. Cartesian coordinates (in Å) of the CASSCF optimized stationary points and conical intersection structures.

Atom	X	Y	Z
		FC	
N	3.572366	2.458976	-1.848652
C	2.425947	2.343528	-2.438129
H	1.505912	2.128394	-1.938064
C	3.768467	2.772876	-4.091394
C	4.452260	2.733539	-2.877348
N	6.390983	3.207963	-4.103103
N	4.316624	3.011174	-5.267516
C	5.625483	3.218822	-5.197707
H	6.126658	3.417895	-6.123134
C	5.818323	2.966158	-2.931244
N	2.462754	2.519858	-3.796402
H	6.442189	2.959787	-2.058959
C	1.359012	2.455076	-4.727427
H	1.527911	1.677661	-5.458086
H	0.455739	2.235624	-4.179151
H	1.242377	3.398949	-5.239575

DOI: 10.1021/ja512536c
J. Am. Chem. Soc. **2015**, S27

Atom	X	Y	Z
		$^{1}(n\pi^*)_{min}$	
N	3.551827	2.452766	-1.828944
C	2.393203	2.336593	-2.429866
H	1.458537	2.120046	-1.939322
C	3.773778	2.768912	-4.052387
C	4.431259	2.725329	-2.839886
N	6.272713	3.193608	-4.135555
N	4.315983	3.015859	-5.300888
C	5.618183	3.229535	-5.282902
H	6.162071	3.434253	-6.194070
C	5.852191	2.960462	-2.836620
N	2.461423	2.517564	-3.780666
H	6.553380	2.974985	-2.026004
C	1.371243	2.456453	-4.730838
H	1.550717	1.669438	-5.459587
H	0.455154	2.243731	-4.188396
H	1.271339	3.406743	-5.249958

Atom	X	Y	Z
		$^{CASSCF}\ ^{1}(\pi\pi^*)_{min}$	
N	3.575664	2.458969	-1.845697
C	2.407972	2.340029	-2.432245
H	1.481214	2.122696	-1.928353
C	3.751074	2.774354	-4.114368
C	4.450445	2.731564	-2.859186
N	6.431309	3.214136	-4.103378
N	4.288763	3.014329	-5.321510
C	5.633658	3.224785	-5.229022
H	6.152340	3.425558	-6.155308
C	5.856210	2.964899	-2.874281
N	2.453703	2.520708	-3.804082
H	6.489821	2.959790	-2.003622
C	1.341967	2.452199	-4.729213
H	1.514063	1.668149	-5.462832
H	0.439146	2.231538	-4.168041
H	1.225662	3.402586	-5.244771

Atom	X	Y	Z
		$^3(n\pi^*)_{min}$	
N	3.557667	2.454453	-1.834514
C	2.398607	2.338241	-2.435281
H	1.465535	2.121610	-1.941146
C	3.776216	2.770229	-4.059136
C	4.437755	2.727336	-2.847139
N	6.281970	3.193810	-4.130343
N	4.316013	3.016559	-5.305875
C	5.606177	3.226970	-5.279758
H	6.156486	3.432537	-6.187970
C	5.854285	2.960368	-2.833365
N	2.460944	2.517935	-3.783158
H	6.545310	2.972507	-2.013791
C	1.368733	2.455962	-4.730065
H	1.546797	1.669263	-5.459642
H	0.454033	2.242404	-4.185472
H	1.266473	3.406093	-5.249232

Atom	X	Y	Z
		$^3(\pi\pi^*)_{min}$	
N	3.619431	2.501523	-1.859211
C	2.374647	2.361349	-2.434203
H	1.469536	2.144621	-1.900268
C	3.740404	2.757668	-4.123019
C	4.432872	2.736515	-2.854144
N	6.433169	3.202104	-4.113326
N	4.269128	2.973692	-5.277137
C	5.680274	3.194971	-5.189919
H	6.163401	3.375471	-6.139303
C	5.879831	2.980796	-2.906327
N	2.436843	2.503725	-3.803875
H	6.506639	2.989524	-2.028831
C	1.332095	2.457853	-4.736334
H	1.578010	1.795620	-5.562346
H	0.455851	2.079626	-4.218391
H	1.120869	3.451217	-5.129251

DOI: 10.1021/ja512536c

Atom	X	Y	Z
	$^{1}(\pi\pi^*/n\pi^*)_{CI}$		
N	3.59030	2.58481	-1.82284
C	2.40750	2.46974	-2.41214
H	1.44114	2.33800	-1.92601
C	3.76019	2.76599	-4.13681
C	4.45158	2.78520	-2.85494
N	6.42737	3.13496	-4.11358
N	4.27172	2.88657	-5.39986
C	5.59600	3.02547	-5.24028
H	6.14371	3.10733	-6.18912
C	5.86275	2.99411	-2.83944
N	2.45760	2.56841	-3.80798
H	6.48690	3.03492	-1.92857
C	1.33057	2.47964	-4.73734
H	1.75502	2.54601	-5.73731
H	0.87563	1.48578	-4.61713
H	0.63492	3.29934	-4.51251

Atom	X	Y	Z
	$^{3}(\pi\pi^*/n\pi^*)_{CI}$		
N	3.56468	2.56397	-1.81817
C	2.36173	2.48496	-2.40494
H	1.41684	2.34403	-1.87921
C	3.76331	2.75947	-4.06828
C	4.42315	2.77014	-2.84193
N	6.33752	3.12809	-4.15370
N	4.29856	2.90610	-5.30476
C	5.65127	3.06912	-5.27954
H	6.19505	3.13603	-6.22356
C	5.84642	3.08057	-2.84994
N	2.43576	2.56017	-3.76759
H	6.53417	2.94616	-2.02740
C	1.36523	2.44415	-4.73992
H	1.80564	2.51863	-5.72962
H	0.81157	1.51094	-4.59147
H	0.68204	3.28375	-4.59584

Atom	X	Y	Z
	$^1(n\pi^*/GS)_{CI}$		
N	3.56816	2.20893	-1.81259
C	2.37647	2.18940	-2.43957
H	1.43028	1.90804	-1.98800
C	3.80828	2.71218	-3.96826
C	4.46772	2.48655	-2.76894
N	6.33888	2.42969	-4.17145
N	4.37543	3.19248	-5.18602
C	5.66896	3.15060	-5.18980
H	6.23439	3.46306	-6.07730
C	5.89014	2.88037	-2.80370
N	2.45530	2.52167	-3.73764
H	6.12580	3.93837	-2.56402
C	1.37611	2.59688	-4.72882
H	1.49929	1.77668	-5.44049
H	0.45932	2.51170	-4.17398
H	1.41850	3.53969	-5.22529

Atom	X	Y	Z
	$^1(\pi\pi^*/GS)_{CI}$		
N	3.61641	2.47842	-1.90575
C	2.42405	2.35433	-2.45480
H	1.52867	2.13277	-1.90959
C	3.71000	2.77740	-4.14559
C	4.42549	2.74163	-2.95283
N	6.44023	2.26616	-4.24096
N	4.33471	3.12927	-5.24847
C	5.70202	3.22831	-4.94066
H	6.28119	3.88590	-5.56261
C	5.86173	2.94075	-3.16421
N	2.40872	2.51806	-3.81734
H	6.51854	3.32389	-2.40673
C	1.27791	2.44614	-4.71269
H	1.40689	1.63501	-5.41970
H	0.38013	2.27355	-4.13670
H	1.17629	3.37471	-5.25728

DOI: 10.1021/ja512536c

Atom	X	Y	Z
	$^1(\pi\pi^*)/^3(n\pi^*)_{ISC}$		
N	3.59013150	2.58472592	-1.82237108
C	2.40743247	2.46961935	-2.41127327
H	1.44116782	2.33800044	-1.92597812
C	3.76028254	2.76651745	-4.14084403
C	4.45277277	2.78510357	-2.85257901
N	6.43146467	3.13539549	-4.11153221
N	4.26788948	2.88595468	-5.39993922
C	5.59539276	3.02522941	-5.23926907
H	6.14372734	3.10733019	-6.18911067
C	5.86162170	2.99413389	-2.84123440
N	2.45788077	2.56856236	-3.80885910
H	6.48695253	3.03492818	-1.92855956
C	1.33056276	2.47964404	-4.73738899
H	1.75504302	2.54603186	-5.73730163
H	0.87562803	1.48577753	-4.61711325
H	0.63494976	3.29932555	-4.51250631

Atom	X	Y	Z
	$^1(n\pi^*)/^3(\pi\pi^*)_{ISC}$		
N	3.567010	2.439630	-1.801890
C	2.378570	2.321860	-2.400500
H	1.425070	2.129540	-1.910530
C	3.754150	2.761580	-4.079660
C	4.429270	2.699480	-2.786620
N	6.273710	3.207380	-4.127780
N	4.283730	3.009540	-5.300020
C	5.656190	3.263610	-5.282990
H	6.188620	3.501220	-6.205330
C	5.895500	2.877560	-2.880790
N	2.452710	2.514560	-3.779850
H	6.571960	3.023210	-2.036580
C	1.367840	2.451130	-4.739610
H	1.514380	1.594470	-5.410190
H	0.430820	2.338600	-4.184420
H	1.352840	3.376230	-5.327860

Tables S5. Cartesian coordinates (in Å) of the stationary points and conical intersection structures optimized by *ab initio* molecular dynamics simulations.

Atom	X	Y	Z
S2/S1 $(n\pi^*)^1/(n\pi^*)^1$			
N	3.4975	2.3863	-2.0212
C	2.3625	2.2334	-2.6166
H	1.454831	1.9467	-2.1277
C	3.6912	2.8106	-4.2756
C	4.3658	2.7829	-3.0246
N	6.1145	3.4826	-4.2863
N	4.2175	2.9350	-5.4600
C	5.5687	3.0474	-5.5036
H	6.0578	3.3295	-6.4085
C	5.7265	3.0110	-3.0553
H	6.4247	2.9024	-2.2516
N	2.3909	2.5102	-3.9663
H	1.6907	2.2712	-4.6296

Atom	X	Y	Z
S3/S2 $(n\pi^*)^1/(\pi\pi^*)^1$			
N	3.4313	2.4913	-1.9969
C	2.3032	2.3638	-2.5669
H	1.3781	2.2109	-2.0474
C	3.6307	2.7311	-4.2906
C	4.3312	2.7131	-3.0273
N	6.1907	3.2382	-4.2980
N	4.1350	2.9574	-5.4695
C	5.4829	3.1939	-5.5033
H	5.9874	3.3946	-6.4130
C	5.6812	3.0173	-3.0643
H	6.3294	3.0955	-2.2117
N	2.3217	2.4741	-3.9360
H	1.5371	2.4549	-4.5440

DOI: 10.1021/ja512536c

Atom	X	Y	Z
S2/T1 $(n\pi^*)^1/(\pi\pi^*)^3$			
N	3.4313	2.4913	-1.9969
C	2.3032	2.3638	-2.5669
H	1.3781	2.2109	-2.0474
C	3.6307	2.7311	-4.2906
C	4.3312	2.7131	-3.0273
N	6.1907	3.2382	-4.2980
N	4.1350	2.9574	-5.4695
C	5.4829	3.1939	-5.5033
H	5.9874	3.3946	-6.4130
C	5.6812	3.0173	-3.0643
H	6.3294	3.0955	-2.2117
N	2.3217	2.4741	-3.9360
H	1.5371	2.4549	-4.5440

Atom	X	Y	Z
T2/T1 $(\pi\pi^*)^3/(n\pi^*)^3$			
N	3.5116	2.4302	-1.9924
C	2.3514	2.2301	-2.5443
H	1.4529	1.9748	-2.0241
C	3.6727	2.6856	-4.2090
C	4.3527	2.7229	-3.0413
N	6.2008	3.1492	-4.3882
N	4.1837	2.9157	-5.4744
C	5.4855	3.1619	-5.5028
H	5.9808	3.3205	-6.4370
C	5.7482	3.1182	-3.0605
H	6.4639	2.8374	-2.3156
N	2.3858	2.3762	-3.9033
H	1.6348	2.2663	-4.5432

DOI: 10.1021/ja512536c

Table S6. MS-CASPT2//CASSCF(16,12)/ANO-L energies (in eV) for the lowest lying singlet and triplet states at the stationary points.

Structure	State	ΔE [eV]	Structure	State	ΔE [eV]
$^1n\pi^*_{MIN}$	S_0	0.672	$^3n\pi^*_{MIN}$	$^3(\pi\pi^*)$	4.076
	$^1(n\pi^*)$	4.018		$^3(n\pi^*)$	4.351
	$^1(\pi\pi^*)$	5.436		$^3(\pi\pi^*)$	4.542
$^1\pi\pi^*_{MIN}$	S_0	0.437	$^3\pi\pi^*_{MIN}$	$^3(\pi\pi^*)$	3.446
	$^1(n\pi^*)$	4.787		$^3(n\pi^*)$	4.208
	$^1(\pi\pi^*)$	4.948		$^3(\pi\pi^*)$	5.237
$(^1\pi\pi^*/n\pi^*)_{CI}$	S_0	0.439	$(^3\pi\pi^*/n\pi^*)_{CI}$	$^3(\pi\pi^*)$	3.861
	$^1(n\pi^*)$	4.851		$^3(n\pi^*)$	3.950
	$^1(\pi\pi^*)$	4.918		$^3(\pi\pi^*)$	4.870
$(^1n\pi^*)/S_0)_{CI}$	S_0	4.616	$(^3\pi\pi^*/S_0)_{CI}$	$^3(\pi\pi^*)$	5.846
	$^1(n\pi^*)$	4.718		$^3(n\pi^*)$	8.239
	$^1(\pi\pi^*)$	6.566		$^3(\pi\pi^*)$	8.679
$(^1\pi\pi^*/ S_0)_{CI}$	S_0	4.933			
	$^1(n\pi^*)$	6.853			
	$^1(\pi\pi^*)$	5.032			
$(^1\pi\pi^*/^3n\pi^*_{CS})_{ISC}$	S_0	0.443	$(^1\pi\pi^*)/^3n\pi^*_{CS})_{ISC}$	$^3(\pi\pi^*)$	4.065
	$^1(n\pi^*)$	4.948		$^3(n\pi^*)$	4.729
	$^1(\pi\pi^*)$	4.881		$^3(\pi\pi^*)$	4.846
$(^1n\pi^*/^3\pi\pi^*_{CS})_{ISC}$	S_0	0.750	$(^1n\pi^*/^3\pi\pi^*_{CS})_{ISC}$	$^3(\pi\pi^*)$	4.100
	$^1(n\pi^*)$	4.053		$^3(n\pi^*)$	3.835
	$^1(\pi\pi^*)$	5.405		$^3(\pi\pi^*)$	5.129

DOI: 10.1021/ja512536c
J. Am. Chem. Soc. **2015**, S35

Table S7. MS-CASPT2 excitation energies and oscillator strengths calculated at particular points along the potential energy surfaces given in Figure 7. These were used to simulate the experimental transient spectra as shown in Figures 8 and S9.

Excited-State	Wavelength (nm)	Oscillator Strength
$S_3(\pi\pi^*)_{FC}$	298	0.0172
	341	0.0142
	352	2E-6
	444	0.0142
	471	2.1E-5
	516	0.0377
	523	2.31E-4
	610	0.0121
	659	0.0102
$S_2(\pi\pi^*)_{FC}$	276	0.00128
	313	0.00356
	322	0.00126
	397	0.041
	410	2.9E-5
	455	0.00664
	459	7.2E-5
	525	0.00622
	561	0.0135
	613	2.9E-5
$S_1(n\pi^*)_{FC}$	288	0.0165
	346	8E-5
	363	1.24E-4
	389	1E-6
	392	8.68E-4
	439	2.58E-4
	464	2.66E-4
	499	0.0246
	582	0.0143
	616	0.0192
$S_2(\pi\pi^*)_{MIN}$	292	0.00182
	305	0.0135
	309	0.0175
	330	0.0406
	356	1.69E-4
	389	1.42E-4
	396	0.0024
	433	2.8E-4
	501	0.00477
	504	0.0245
	593	0.00706
	613	0.0115
	659	2.95E-4
	696	2.05E-4
$S_1(n\pi^*)_{UR}$	280	7.8E-5
	292	0.012
	296	0.00985
	315	0.00892
	337	2.32E-4
	369	8.36E-4
	374	9.3E-5
	409	0.00967
	466	0.00414
	469	8.06E-4
	546	5.39E-4
	563	2.73E-4
	598	0.0187
	632	0.0104
$S_1(n\pi^*)_{R}$	266	0.00117
	303	4.8E-5
	307	0.0244
	313	1E-6
	322	1.34E-4
	379	3.46E-4
	399	0.00286
	420	0.0191
	427	4E-6
	438	0.0105
	454	1.8E-5
$T_2(\pi\pi^*)$	287	0.00356
	307	0.0235
	334	0.0177
	335	4.42E-4
	372	1.26E-4
	420	1.44E-4
	460	0.00458
	464	1.5E-5
	493	0.0576
	539	3E-6
	582	0.0079
$T_1(\pi\pi^*)_{MIN}$	407	0.00717
	461	1.78E-5
	553	0.00153
	556	0.00553
	606	5.01E-5
	724	0.00835

III. REFERENCES

(1) Mason, S. F. *J. Chem. Soc.* **1954**, 2071.
(2) Voet, D.; Gratzer, W. B.; Cox, R. A.; Doty, P. *Biopolymers* **1963**, *1*, 193.
(3) Clark, L. B.; Tinoco, I. *J. Am. Chem. Soc.* **1965**, *87*, 11.
(4) Drobnik, J.; Augenstein, L. *Photochem. Photobiol.* **1966**, *5*, 13.
(5) Chen, H. H.; Clark, L. B. *J. Chem. Phys.* **1969**, *51*, 1862.
(6) Albinsson, B.; Nordén, B. *J. Am. Chem. Soc.* **1993**, *115*, 223.
(7) Borin, A. C.; Serrano-Andrés, L. *J. Phys. Chem. A* **1999**, *103*, 1838.
(8) Catalán, J. *Chem. Phys.* **2004**, *303*, 205.
(9) Mburu, E.; Matsika, S. *J. Phys. Chem. A* **2008**, *112*, 12485.
(10) Gonnella, N. C.; Roberts, J. D. *J. Am. Chem. Soc.* **1982**, *1982*, 3162.
(11) Schumacher, M.; Günther, H. *J. Am. Chem. Soc.* **1982**, *104*, 4167.
(12) Majoube, M.; Henry, M.; Vergoten, G. *J. Raman Spectrosc.* **1994**, *25*, 233.
(13) Majoube, M.; Millié, P.; Chinsky, L.; Turpin, P. Y.; Vergoten, G. *J. Mol. Struct.* **1995**, *355*, 147.
(14) Broo, A.; Holmén, A. *Chem. Phys.* **1996**, *211*, 147.
(15) Ten, G. N.; Burova, T. G.; Baranov, V. I. *Russian Phys. J.* **2004**, *47*, 626.
(16) Nowak, M. J.; Rostkowaska, H.; Lapinski, L.; Kwiatkowski, J. S.; Leszczynski, J. *Spectrochim. Acta* **1994**, *50A*, 1081.
(17) Nowak, M. J.; Rostkowaska, H.; Lapinski, L.; Kwiatkowski, J. S.; Leszczynski, J. *J. Phys. Chem.* **1994**, *98*, 2813.
(18) Ha, T.-K.; Keller, M. J.; Gunde, R.; Gunthard, H. H. *J. Mol. Struct. (Theochem)* **1996**, *364*, 161.
(19) Caminati, W.; Maccaferri, G.; Favero, P. G.; Favero, L. B. *Chem. Phys. Lett.* **1996**, *251*, 189.
(20) Schneider, M.; Hain, T.; Fischer, I. *ChemPhysChem* **2009**, *10*, 634.
(21) Middleton, C. T.; de La Harpe, K.; Su, C.; Law, Y. K.; Crespo-Hernández, C. E.; Kohler, B. *Annu. Rev. Phys. Chem.* **2009**, *60*, 217.
(22) Crespo-Hernández, C. E.; Cohen, B.; Hare, P. M.; Kohler, B. *Chem. Rev.* **2004**, *104*, 1977.
(23) Quiñones, E.; Arce, R. *J. Am. Chem. Soc.* **1989**, *111*, 8218.
(24) Reichardt, C.; Vogt, R. A.; Crespo-Hernández, C. E. *J. Chem. Phys.* **2009**, *131*, 224518.
(25) Reichardt, C.; Wen, C.; Vogt, R.; Crespo-Hernández, C. *Photochem. and Photobiol. Sci.* **2013**, *12*, 1341.
(26) Reichardt, C.; Wen, C.; Vogt, G.; Crespo-Hernández, C. E. *Photochem. Photobiol. Sci.* **2013**, *12*, 2203.
(27) Trebino, R.; DeLong, K. W.; Fittinghoff, D. N.; Sweetser, J. N.; Krumbügel, M. A.; Richman, B. A.; Kane, D. J. *Rev. Sci. Instrum.* **1997**, *68*, 3277.
(28) Maciejewski, A.; Naskrecki, R.; Lorenc, M.; Ziolek, M.; Karolczak, J.; Kubicki, J.; Matysiak, M.; Szymanski, M. *J. Mol. Struc.* **2000**, *555*, 1.
(29) Lorenc, M.; Ziolek, M.; Naskrecki, R.; Karolczak, J.; Kubicki, J.; Maciejewski, A. *Appl. Phys. B: Laser Opt.* **2002**, *87*, 2340.
(30) Crespo-Hernández, C. E.; Kohler, B. *J. Phys. Chem. B* **2004**, *108*, 11182.
(31) Vogt, R. A.; Gray, T. G.; Crespo-Hernández, C. E. *J. Am. Chem. Soc.* **2012**, *134*, 14808.
(32) van Stokkum, I. H. M.; Larsen, D. S.; van Grondelle, R. *Biochim. Biophys. Acta* **2004**, *1657*, 82.
(33) van Stokkum, I. H. M.; Larsen, D. S.; van Grondelle, R. *Biochim. Biophys. Acta* **2004**, *1658*, 262.
(34) Capellos, C.; Bielski, B. H. J. *Kinetic Systems*; Wiley Interscience: New York, 1972.
(35) Lakowicz, J. R. *Prinicples of Fluorescence Spectroscopy*; 3rd ed.; Springer, 2006.
(36) Onidas, D.; Markovitsi, D.; Marguet, S.; Sharonov, A.; Gustavsson, T. *J. Phys. Chem. B* **2002**, *106*, 11367.
(37) Frisch, M. J.; Trucks, G. W.; Schlegel, H. B.; Scuseria, G. E.; Robb, M. A.; Cheeseman, J. R.; Zakrzewski, V. G.; Montgomery Jr., J. A.; Stratmann, R. E.; Burant, J. C.; Dapprich, S.; Millam, J. M.; Daniels, K. N.; Kudin, K. N.; Strain, M. C.; Farkas, O.; Tomasi, J.; Barone, V.; Cossi, M.; Cammi, R.; Mennucci, B.; Pomelli, C.; Adamo, C.; Clifford, S.; Ochterski, J.; Petersson, G. A.; Ayala, P. Y.; Cui, Q.; Morokuma, K.; Malick, D. K.; Rabuck, A. D.; Raghavachari, K.; Foresman, J. B.; Cioslowski, J.; Ortiz, J. V.; Baboul, A. G.; Stefanov, B. B.; Liu, G.; Liashenko, A.; Piskorz, P.; Komaromi, I.; Gomperts, R.; Martin, R. L.; Fox, D. J.; Keith, T.; Al-Laham, M. A.; Peng, C. Y.; Nanayakkara, A.; Gonzalez, C.; Challacombe, M.; Gill, P. M. W.;

DOI: 10.1021/ja512536c
J. Am. Chem. Soc. **2015**, S37

Johnson, B. G.; Chen, W.; Wong, M. W.; Andres, J. L.; Head-Gordon, M.; Replogle, E. S.; Pople, J. A.; Gaussian, Inc.: Wallingford CT: Pittsburgh, PA, 2004.
(38) Adamo, C.; Barone, V. *J. Chem. Phys.* **1999**, *110*, 6158.
(39) Improta, R.; Barone, V.; Santoro, F. *J. Phys. Chem. B* **2007**, *111*, 14080.
(40) Jacquemin, D.; Wathelet, V.; Perpète, E. A.; Adamo, C. *J. Chem. Theory Compt.* **2009**, *5*, 2420.
(41) Fabiano, E.; Della Sala, F.; Barbarella, G.; Lattante, S.; Anni, M.; Sotgiu, G.; Hättig, C.; Cingolani, R.; Gigli, G. *J. Phys. Chem. B* **2006**, *110*, 18651.
(42) Mennucci, B.; Toniolo, A.; Tomasi, J. *J. Phys. Chem. A* **2001**, *105*, 4749.
(43) Improta, R.; Scalmani, G.; Frisch, M. J.; Barone, V. *J. Chem. Phys.* **2007**, *127*, 074504.
(44) Barone, V.; Cossi, M.; Tomasi, J. *J. Chem. Phys.* **1997**, *107*, 3210.
(45) Cancès, E.; Mennucci, B.; Tomasi, J. *J. Chem. Phys.* **1997**, *107*, 3032.
(46) Roos, B. O. *Ab Initio Methods in Quantum Chemistry*; Wiley: Chichester, 1987; Vol. II.
(47) Widmark, P.-O.; Malmquist, P.-Å.; Roos, B. O. *Theor. Chim. Acta* **1990**, *77*, 291.
(48) Andersson, K.; Malmquist, P.-Å.; Roos, B. O. *J. Chem. Phys.* **1992**, *96*, 1218.
(49) Finley, J.; Malmqvist, P.-A.; Roos, B. O.; Serrano-Andrés, L. *Chem. Phys. Lett.* **1998**, *288*, 299.
(50) Roos, B. O.; Andersson, K. *Chem. Phys. Lett.* **1995**, *245*, 215.
(51) Ghigo, G.; Roos, B. O.; Malmquist, P.-Å. *Chem. Phys. Lett.* **2004**, 142.
(52) Aquilante, F.; De Vico, L.; Ferré, N.; Ghigo, G.; Malmqvist, P.-A.; Neogrády, P.; Pedersen, T. B.; Pitonák, M.; Reiher, M.; Roos, B. O.; Serrano-Andrés, L.; Urban, M.; Veryazov, V.; Lindh, R. *J. Comput. Chem.* **2010**, *31*, 224.
(53) Werner, H.-J.; Knowles, P. J.; Lindh, R.; Manby, F. R.; Schütz, M.; Celani, P.; Korona, T.; Mitrushenkov, A.; Rauhut, G.; Adler, T. B.; Amos, R. D.; Bernhardsson, A.; Berning, A.; Cooper, D. L.; Deegan, M. J. O.; Dobbyn, A. J.; Eckert, F.; Goll, E.; Hampel, C.; Hetzer, G.; Hrenar, T.; Knizia, G.; Köppl, C.; Liu, Y.; Lloyd, A. W.; Mata, R. A.; May, A. J.; McNicholas, S. J.; Meyer, W.; Mura, M. E.; Nicklass, A.; Palmieri, P.; Pflüger, K.; Pitzer, R.; Reiher, M.; Schumann, U.; Stoll, H.; Stone, A. J.; Tarroni, R.; Thorsteinsson, T.; Wang, M.; Wolf, A.; MOLPRO, version 2009.1. http://www.molpro.net.
(54) *Photodissociation Dynamics: Spectroscopy and Fragmentation of Small Polyatomic Molecules*; Cambridge University Press, 1995.
(55) Dahl, J. P.; Springborg, M. *J. Chem. Phys.* **1988**, *88*, 4535.
(56) Weigend, F.; Ahlrichs, R. *Phys. Chem. Chem. Phys.* **2005**, *7*, 3297.
(57) Barbatti, M.; Granucci, G.; Persico, M.; Ruckenbauer, M.; Vazdar, M.; Eckert-Maksić, M.; Lischka, H. *J. Photochem. Photobiol A* **2007**, *190*, 228.
(58) Newton-X. http://www.newtonx.org: 2014.
(59) Richter, M.; Marquetand, P.; González-Vázquez, J.; Sola, I.; González, L. *J. Chem. Theory Compt.* **2011**, *7*, 1253.
(60) Mai, S.; Richter, M.; Ruckenbauer, M.; Oppel, M.; Marquetand, P.; González, L. SHARC: Surface Hopping Including Arbitrary Couplings – Program Package for Non-Adiabatic Dynamics. http://sharc-md.org: 2014.
(61) Werner, H.-J.; Knowles, P. J.; Knizia, G.; Manby, F. R.; Schütz, M. *WIREs Comput. Mol. Sci.* **2012**, *2*, 242.
(62) Kwiatkowski, J. S. *Theor. Chim. Acta* **1968**, *10*, 47.

DOI: 10.1021/ja512536c
J. Am. Chem. Soc. **2015**, S38